CHEMICAL ABUNDANCES OF THE DAMPED Ly α SYSTEMS AT Z>1.5

JASON X. PROCHASKA¹ & ARTHUR M. WOLFE¹
DEPARTMENT OF PHYSICS, AND CENTER FOR ASTROPHYSICS AND SPACE SCIENCES;
UNIVERSITY OF CALIFORNIA, SAN DIEGO;
C-0424; LA JOLLA; CA 92093

ApJ: Accepted October 20, 1998

ABSTRACT

We present chemical abundance measurements for 19 damped Ly α systems observed with HIRES on the 10m W.M. Keck Telescope. We perform a detailed analysis of every system, deriving ionic column densities for all unblended metal-line transitions. Our principal goal is to investigate the abundance patterns of the damped systems and thereby determine the underlying physical processes which dominate their chemical evolution. We place particular emphasis on gauging the relative importance of two complementary effects often invoked to explain the damped Ly α abundances: (1) nucleosynthetic enrichment from Type II supernovae and (2) an ISM-like dust depletion pattern.

Similar to the principal results of Lu et al. (1996), our observations lend support both for dust depletion and Type II SN enrichment. Specifically, the observed overabundance of Zn/Fe and underabundance of Ni/Fe relative to solar abundances suggest significant dust depletion within the damped Ly α systems. Meanwhile, the relative abundances of Al, Si, and Cr vs. Fe are consistent with both dust depletion and Type II supernova enrichment. Our measurements of Ti/Fe and the Mn/Fe measurements from Lu et al. (1996), however, cannot be explained by dust depletion and indicate an underlying Type II SN pattern. Finally, the observed values of [S/Fe] are inconsistent with the combined effects of dust depletion and the nucleosynthetic yields expected for Type II supernovae. This last result emphasizes the need for another physical process to explain the damped Ly α abundance patterns.

We also examine the metallicity of the damped Ly α systems both with respect to Zn/H and Fe/H. Our results confirm previous surveys by Pettini and collaborators, i.e., $[<\text{Zn/H}>] = -1.15 \pm 0.15$ dex. In contrast with other damped Ly α surveys at z>1.5, we do not formally observe an evolution of metallicity with redshift, although we stress this result is based on the statistics from a small sample of high z damped systems.

Subject headings: cosmology: observations — galaxies: abundances — galaxies: chemical evolution — quasars: absorption lines — nucleosynthesis

1. INTRODUCTION

The damped Ly α systems dominate the neutral gas content of the universe and at high redshift are widely believed to be the progenitors of present-day galaxies (Wolfe et al. 1995). Therefore, one can directly measure the chemical evolution of the early universe by tracing the chemical abundances of the damped systems. Pettini and his collaborators have performed the most extensive surveys on the metallicity of the damped $Lv\alpha$ systems to date (Pettini et al. 1994, Pettini et al. 1997). Working on the premise one can measure accurate column densities of Zn⁺ and Cr⁺ from unresolved line profiles, they have successfully observed over 30 damped Ly α systems with the Anglo-Australian, William Herschel, and Hale Telescopes. Their results indicate a mean metallicity of $Zn/H \approx 1/10$ solar abundance with a notably large dispersion. These measurements indicate the damped systems are chemically young at z > 2 and lend further support to the interpretation of damped systems as the progenitors of modern galaxies (e.g. Malaney and Chaboyer 1996). In addition to an analysis of Zn, Pettini et al. performed accurate measurements of $N(Cr^+)$ aided by the coincidence in wavelength of the strongest metal-line transitions for the two species. Comparing the relative abundances of Cr and Zn,

¹Visiting Astronomer, W.M. Keck Telescope. The Keck Observatory is a joint facility of the University of California and the California Institute of Technology.

they noted an underabundance of Cr to Zn relative to solar abundances (a typical value² is $[Cr/Zn] \approx -0.5$ dex). In the ISM, Cr is significantly depleted onto dust grains while Zn is only lightly depleted. Therefore, Pettini and others have argued that the relative underabundance of Cr to Zn is indicative of dust in the damped Ly α systems. They also point out the Cr/Zn measurements imply a dust-to-gas ratio much lower than that observed in dusty ISM regions where typical values for [Cr/Zn] are less than -1.0 dex. Establishing the level of dust depletion in damped Ly α systems is very important as dust could significantly bias the results from the damped Ly α surveys against high N(HI) systems (Fall & Pei 1993).

More recently, Lu et al. (1996) have offered an alternate interpretation for the abundance patterns of the damped systems. Unlike the Pettini et al. sample, Lu et al. measured abundances for a large number of elements including Zn, Cr, Fe, S, N, O, Si, Ni, and Mn with HIRES on the 10m W.M. Keck Telescope. The primary result of their analysis is that the damped Ly α systems exhibit abundance patterns typical of nucleosynthetic yields for Type II supernova. The tell-tale signature of Type II SN enrichment is the overabundance of α -process elements (e.g. Si and S) relative to Fe. Empirical measurements of the abundance patterns for Type II SN are commonly derived from the metal-poor halo stars (Evardsson et al. 1993)

 $^{2}[X/Y] \equiv \log[X/Y] - \log[X/Y]_{\odot}$

QSO	Alternate Name	Date Time (s)	Exposure	$\frac{z_{em}}{(\text{km s}^{-1})}$	Resolution	SNR
-		\ /				
Q0019 - 15	BR $0019-1522$	F96	35000	4.528	7.5	18
Q0100+13	PHL 957	S94	11700	2.69	7.5	40
Q0149+33	OC 383	F97	17600	2.43	7.5	25
Q0201 + 36	UT 0201+3634	F94	34580	2.49	7.5	35
Q0347 - 38		F96	12600	3.23	7.5	33
Q0458 - 02	PKS 0458-020	F95	28800	2.29	7.5	15
Q0841+12	•••	F97,S98	10800		7.5	30
Q0951 - 04	BR $0951 - 0450$	S97	30600	4.369	7.5	13
Q1215+33	$GC\ 1215+3322$	S94	14040	2.61	7.5	20
Q1331+17	MC 1331+170	S94	36000	2.08	6.6	80
Q1346 - 03	BRI 1346-0322	S97	31000	3.992	7.5	29
Q1759 + 75	GB1759 + 7539	F96	10400	3.05	6.6	33
Q2206-19		F94	25900	2.56	7.5	40
Q2230+02	LBQS 2230+0232	F97	18000	2.15	7.5	26
Q2231-00	LBQS 2230-0015	F95	14400	3.02	7.5	30
Q2348-14		F96	9000	2.940	7.5	41
Q2359 - 02	UM 196	F97	25000	2.31	7.5	17

TABLE 1
QSO AND OBSERVATIONAL DATA

which presumably were primarily enriched by Type II supernova. As expected for Type II SN abundances, Lu et al. found an overabundance of Si/Fe in every case and further noted that the relative abundances of Fe, Cr, Mn, N, O, and S all match the metal-poor halo star observations. Furthermore, Lu et al. stress the measured ratios of Mn/Fe and N/O cannot be explained in terms of dust depletion and therefore argue for an underlying Type II SN abundance pattern. The interpretation of the damped Ly α abundances patterns as Type II SN enrichment fails, however, with respect to Zn. In particular, the observed overabundance of Zn to Fe (or Cr) contradicts the observations of halo stars where one finds $[Zn/Fe] \approx 0 \text{ dex}$ irrespective of the star's metallicity. While it is possible to theoretically explain the observed overabundance of Zn relative to Fe as a natural consequence of Type II supernova enrichment (Hoffman et al. 1996), the halo star observations pose a significant problem. Several authors have interpreted the observed abundance patterns by combining the effects of dust depletion and Type II SN enrichment (Lu et al. 1996, Kulkarni et al. 1997, Vladilo 1998), but their efforts have been largely unsuccessful. They have had particular difficulty in matching both the [Zn/Fe] and [Mn/Fe] patterns observed in the damped systems. Developing a consistent explanation for all of the abundance patterns remains an outstanding problem.

In this paper, we investigate these issues with observations of 19 damped Ly α systems, including two systems previously observed by Lu et al. (1996). Building on the abundance results from Prochaska & Wolfe (1996) and Prochaska & Wolfe (1997a), we derive ionic column densities for all of the unblended metal-line transitions comprising our damped Ly α sample. In turn, we look for abundance patterns similar to those observed in the Lu et al. (1996) sample and also interpret these results in the light

of dust depletion. Lastly, we investigate the evolution of the observed metallicity of the damped Ly α systems with increasing redshift.

In § 2 we summarize the observational sample and data reduction techniques. The individual damped systems are briefly discussed in § 3 and measurements of the ionic column densities and velocity plots of the metal-line transitions are presented. § 4 discusses the observed abundance patterns of the damped Ly α systems. Finally, the metallicity of the damped Ly α systems is investigated in § 5 and a brief summary is given in § 6.

2. OBSERVATIONAL SAMPLE

Table 1 presents a journal of our observations. In addition to exposure times and dates, we estimate the typical signal-to-noise ratio per pixel (SNR) and resolution of the spectra, and include the emission redshift, z_{em} , of the quasar. All of the data were acquired with the high-resolution echelle spectrograph (HIRES; Vogt 1992) on the 10m W.M. Keck I telescope. The data were reduced with the HIRES software package developed by T. Barlow. This package converts the 2D echelle images to fully reduced, 1D wavelength-calibrated spectra. We then continuum fit these spectra with a program similar to the IRAF package continuum and optimally coadded multiple observations.

Our observational sample of QSO's all have at least one known intervening damped Ly α system. The systems exhibit a range of $N({\rm HI})$ values and absorption redshifts ($z_{abs}=1.8-4.2$). In several cases, we have identified additional metal-line systems with very large ionic column densities which suggest they are damped systems. In the following, however, we restrict our analysis to systems with measured HI column density, $N({\rm HI}) > 2 \times 10^{20} \, {\rm cm}^{-2}$. The metal-line transitions are identified by composing velocity plots of the absorption lines listed in Table 2 at the

Table 2
Metal Line Data

Transition	$\lambda_{\mathrm{rest}} (\mathring{A})$	f^a
HI 1215	1215.6701	0.4164
OI 1302	1302.1685	0.04887
SiII 1304	1304.3702	0.0940
NiII 1317	1317.217	0.1458^{b}
CII 1334	1334.5323	0.1278
CuII 1358	1358.773	0.3803
NiII 1370	1370.131	0.144
SiIV 1393	1393.755	0.528
SnII 1400	1400.400	0.71
SiIV 1402	1402.770	0.262
GaII 1414	1414.402	1.8
NiII 1454	1454.842	0.0516
SiII 1526	1526.7066	0.1160
CIV 1548	1548.195	0.1908
CIV 1550	1550.770	0.09522
GeII 1602	1602.4863	0.135
FeII 1608	1608.4511	0.06196
FeII 1611	1611.2005	0.001020
AlII 1670	1670.7874	1.88
PbII 1682	1682.15	0.156
NiII 1703	1703.405	0.01224
NiII 1709	1709.600	0.0666^{b}
NiII 1741	1741.549	0.0776^{b}
NiII 1751	1751.910	0.0638
SiII 1808	1808.0126	0.00218
AlIII 1854	1854.716	0.539
AlIII 1862	1862.790	0.268
TiII 1910a	1910.6	0.0975
TiII 1910b	1910.97	0.0706
ZnII 2026	2026.136	0.489
$CrII\ 2056$	2056.254	0.1050^{c}
$CrII\ 2062$	2062.234	0.0780^{c}
ZnII 2062	2062.664	0.256
$CrII\ 2066$	2066.161	0.05150^{c}
FeII 2260	2260.7805	0.00244
FeII 2344	2344.214	0.1108
FeII 2374	2374.4612	0.03260
FeII 2382	2382.765	0.3006
MnII 2576	2576.877	0.3508
FeII 2586	2586.6500	0.0684
MnII 2594	2594.499	0.2710
FeII 2600	2600.1729	0.2132
MnII 2606	2606.462	0.1927

 a Unless otherwise indicated, the f and λ values were taken from Morton (1991) b Zsargo & Federman (1998) c Tripp et al. (1996)

known redshift of the damped system and then correlating the profiles by eye. We performed a systematic search for other metal-line systems toward each QSO to account for possible line misidentification and blending. The data are presented in the following section.

3. IONIC COLUMN DENSITIES

All of the ionic column densities presented in this section were derived with the apparent optical depth method (AODM; Savage and Sembach 1991). Savage and Sembach (1991) have stressed measuring column densities by fitting multiple Voigt profiles to the line-profiles does not always account for hidden saturated components. They introduced a technique to correct for hidden saturation by comparing the apparent column density, N_a , for multiple transitions from a single ion. The analysis involves calculating $N_a(v)$ for each pixel from the optical depth equation

$$N_a(v) = \frac{m_e c}{\pi e^2} \frac{\tau_a(v)}{f \lambda},\tag{1}$$

where $\tau_a(v) = \ln[I_i(v)/I_a(v)]$, f is the oscillator strength, λ is the rest wavelength and I_i and I_a are the incident and measured intensity. Comparing $N_a(v)$ deduced from two or more transitions of the same ion, one finds the stronger transition will have smaller values of $N_a(v)$ in those features where hidden saturation is present. Thus, one can ascertain the likelihood of saturated components for ions with multiple transitions.

In Wolfe et al. (1994), Prochaska & Wolfe (1996) and Prochaska & Wolfe (1997a), we showed the damped Ly α profiles are not contaminated by hidden saturation. Furthermore, we demonstrated the column densities derived with the AODM agree very well with line-profile fitting, which should give a more accurate measure of the ionic column densities when hidden saturation is negligible. As the AODM is easier to apply to a large data set, we have chosen to use this technique to measure the ionic column densities for the damped Ly α sample. Throughout the paper we adopt the wavelengths and oscillator strengths presented in Table 2 compiled by Morton (1991), Tripp et al. (1996), and Zsargó & Federman (1998).

Tables 3–21 present the results of the abundance measurements including an estimate of the 1σ error. For those transitions where the profile saturates (i.e. $I_i/I_a < 0.01$ in at least one pixel), the column densities are listed as lower limits. The values reported as upper limits are 3σ upper limits. We warn the reader of two points: (1) logarithmic errors are misleadingly small (e.g. a 0.1 dex error is $\approx 25\%$ for a 13 dex measurement) and (2) we have ignored continuum error in our analysis which could significantly affect measurements of very weak transitions. In the following subsections we comment briefly on each of the damped Ly α systems, plot all of the identified metal-line transitions, and discuss the adopted $N(\mathrm{HI})$ values. We note which systems are members of the LBQS sample (Wolfe et al. 1995) and advise the reader the refer to that paper for further details. In the velocity plots, v=0 is chosen arbitrarily and corresponds to the redshift listed in the figure caption. We indicate regions where blends with other transitions occur (primarily through blends with other metalline systems or the Ly α forest) by plotting with dotted lines.

3.1. Q0000-26, z=3.390

This high redshift damped Ly α system has been previously observed with HIRES (Lu et al. 1996) and we adopt $\log N(\mathrm{HI}) = 21.41 \pm 0.08$ based on that analysis. It is a member of the LBQS (Wolfe et al. 1995) statistical sample, one of the few with $z_{abs} > 3$ The velocity profiles are presented in Figure 1 and the derived ionic column densities are listed in Table 3. As our spectral coverage did not include FeII 1608, the Fe abundance is based solely on FeII 1611 which is a very weak transition and has a relatively low SNR. Interestingly, we find $N(\text{Fe}^+)$ to be significantly higher than the lower limit derived from the FeII 1608 transition reported by Lu et al. (1996), which may be the result of an error in the continuum fit to our profile. We find $N(Si^+)$ to be significantly higher as well, however, both from the direct measurement of the SiII 1808 transition and by fitting a Voigt profile to the saturated SiII 1526 profile. We therefore note Lu et al. (1996) may have significantly underestimated the true metallicity. At the same time, we observe that the $N(Ni^+)$ measurement coincides with the Lu et al. results. Because we have no unblended, unsaturated high SNR profiles for this system we have not included it in the kinematic analyses thus far (Prochaska & Wolfe 1997b, Wolfe & Prochaska 1998, Prochaska & Wolfe 1998).

Table 3 $\label{eq:table 3} \mbox{Ionic Column Densities: } Q0000-26,\,z=3.390$

Ion	١	AODM	M	[V /H]
1011		AODM	N_{adopt}	[A/11]
$_{ m HI}$	1215	21.410 ± 0.080		
CIV	1548	14.707 ± 0.006		
AlIII	1854	12.772 ± 0.020		
SiII	1526	> 14.607	15.086 ± 0.012	-1.874 ± 0.081
	1808	15.086 ± 0.012		
FeII	1611	15.146 ± 0.037	15.146 ± 0.037	-1.774 ± 0.088
NiII	1751	13.325 ± 0.029	13.325 ± 0.029	-2.335 ± 0.085

3.2.
$$Q0019-15$$
, $z = 3.439$

This damped Ly α system comes from the high redshift survey by Storrie-Lombardi et al. (1996) and the adopted $\log N({\rm HI}) = 20.9 \pm 0.1$ was taken from recent Keck measurements of Storrie-Lombardi & Wolfe (1998). While our observations covered Ly α for this system, the profile extends over two echelle orders and an accurate measurement of $N({\rm HI})$ proved impossible. Figure 2 shows the metal-line transitions and Table 4 presents the measurements for this system. The Fe abundance is based on the marginally saturated FeII 1608 profile, yet should be reasonably accurate. The NiII lines are very weak and in poor SNR regions so these measurements are not reliable. The same is true for the Si measurements, although to a lesser extent. Note all of the high-ion profiles are blended with other metal-line transitions or Ly α forest clouds.

3.3.
$$Q0100+13$$
, $z=2.309$

The majority of our results on PHL 957 (a.k.a. Q0100+13) were published by Wolfe et al. (1994). The major exception is we now present a measurement of the Fe abundance based on the previously unidentified FeII 1611 profile. Also, we measure column densities in light of new f

5

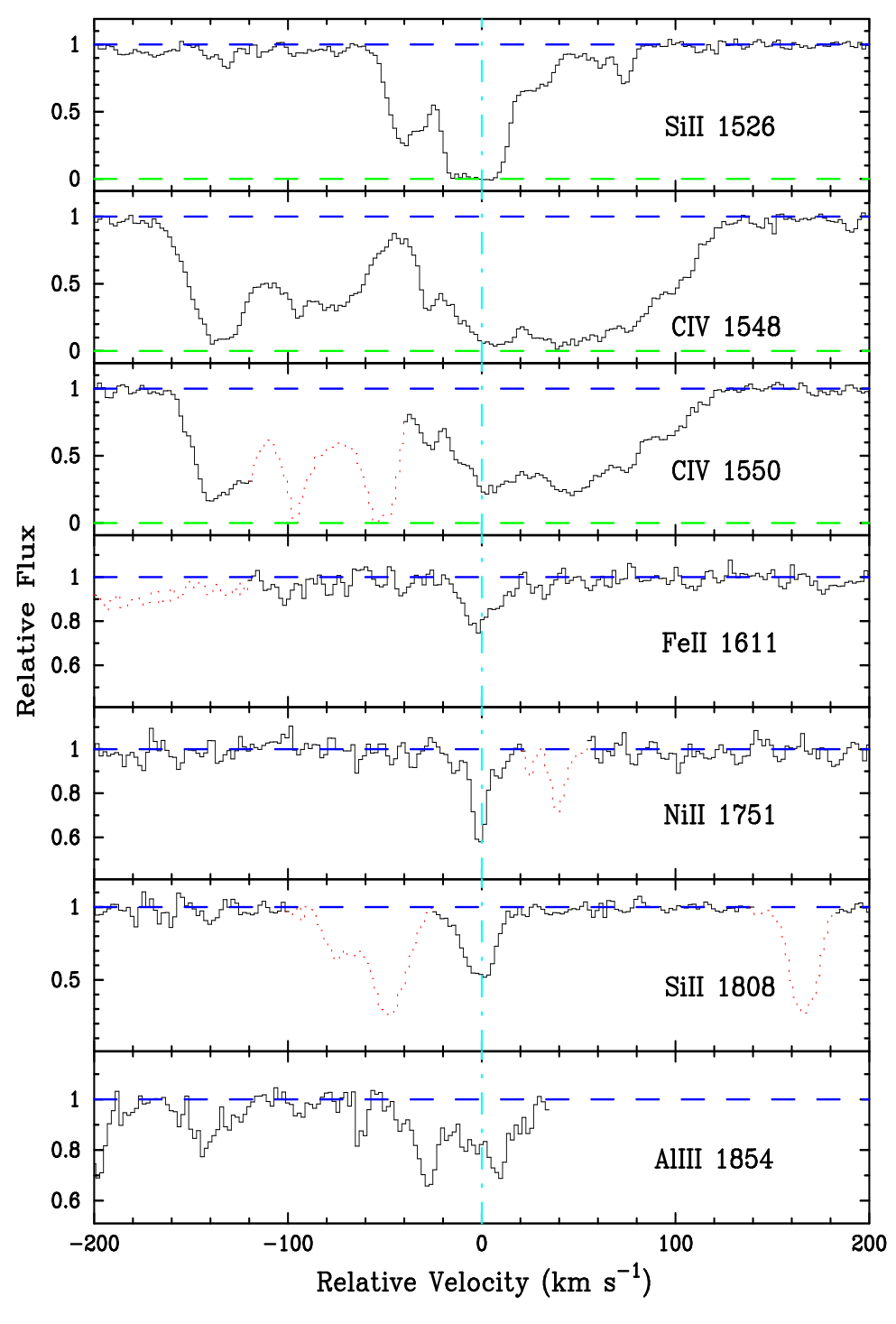


Fig. 1.— Velocity plot of the metal-line transitions for the damped Ly α system at z=3.390 toward Q0000–26. The vertical line at v=0 corresponds to z=3.3901. Figures 2-21 are not included here but can be downloaded from: http://mamacass.ucsd.edu:8080/people/xavier/WWW/DLA/abundfig.ps.gz

 $\label{eq:table 4} \text{Ionic Column Densities: } Q0019-15,\,z=3.439$

Ion	λ	AODM	N_{adopt}	[X/H]
HI SiII	1215 1526 1808	20.900 ± 0.100 > 14.953 15.423 ± 0.053	15.423 ± 0.053	-1.027 ± 0.113
SiIV FeII NiII	1402 1608 1709 1741	> 14.495 14.770 ± 0.064 13.300 ± 0.103 13.442 ± 0.043	14.770 ± 0.064 13.442 ± 0.043	$-1.640 \pm 0.119 \\ -1.708 \pm 0.109$

and λ values, in particular those for the CrII and NiII transitions. Note the O abundance is based on the very weak OI 1355 profile and we report it as a 3σ upper limit. Figure 3 presents the velocity plots and Table 5 lists the measured ionic column densities for this system. This damped system is included in the statistical sample of the LBQS survey.

 $\label{eq:table 5} \text{Ionic Column Densities: } Q0100+13,\,z=2.309$

Ion	λ	AODM	N_{adopt}	[X/H]
HI	1215	21.400 ± 0.050		
CIV	1548	13.241 ± 0.031		
	1550	13.303 ± 0.056		
OI	1355	< 17.628	< 17.628	< -0.702
AlIII	1854	12.635 ± 0.022		
	1862	12.715 ± 0.033		
SiII	1526	> 14.722	> 14.722	> -2.228
SiIV	1393	13.127 ± 0.017		
	1402	13.146 ± 0.029		
CrII	2062	13.389 ± 0.018	13.387 ± 0.015	-1.693 ± 0.052
	2066	13.383 ± 0.024		
FeII	1608	> 14.599	15.096 ± 0.041	-1.814 ± 0.065
	1611	15.096 ± 0.041		
NiII	1454	13.621 ± 0.041	13.620 ± 0.014	-2.030 ± 0.052
	1741	13.620 ± 0.015		
ZnII	2026	12.498 ± 0.028	12.494 ± 0.023	-1.556 ± 0.055
	2062	12.485 ± 0.039		

3.4.
$$Q0149+33$$
, $z=2.140$

This relatively metal-poor ([Fe/H] ≈ -1.8 dex) damped system is a also member of the LBQS statistical sample. Table 6 gives the measured column densities and Figure 4 plots the metal-lines. In the following analysis, we assume $\log N({\rm HI}) = 20.5 \pm 0.1$ (Wolfe et al. 1995). As with PH957, the O abundance is based on the statistically insignificant OI 1355 profile and provides a very conservative upper limit. Finally the Al abundance is derived from the marginally saturated AlII 1670 profile but should be a reliable value. The system is notable for exhibiting an atypical Cr to Zn ratio; $[Cr/Zn] = +0.26 \pm 0.1$ dex. The Cr measurement is reasonably accurate and the ZnII 2062 transition places a rather strict upper limit to the Zn abundance. Therefore, it is very likely [Cr/Zn] > 0 which marks the first such occurrence in a damped system and indicates this system must be essentially undepleted.

3.5.
$$Q0347-38$$
, $z = 3.025$

 $\label{eq:Table 6} \text{Ionic Column Densities: Q0149+33, } z = 2.140$

Ion	λ	AODM	N_{adopt}	[X/H]
HI	1215	20.500 ± 0.100		
$_{\rm CI}$	1560	< 12.801		
CII	1334	> 14.623		
	1335	< 12.780		
CIV	1548	13.880 ± 0.011		
	1550	13.890 ± 0.017		
OI	1355	< 17.795	< 17.795	< 0.365
AlII	1670	12.936 ± 0.018	12.936 ± 0.018	-2.044 ± 0.102
AlIII	1854	12.518 ± 0.028		
	1862	12.556 ± 0.043		
SiII	1304	14.401 ± 0.042	14.367 ± 0.029	-1.683 ± 0.104
	1526	14.320 ± 0.034		
	1808	14.572 ± 0.047		
SiIV	1393	13.380 ± 0.017		
CrII	2056	12.793 ± 0.044	12.811 ± 0.036	-1.369 ± 0.106
	2062	12.533 ± 0.087		
	2066	12.853 ± 0.060		
$_{\mathrm{FeII}}$	1608	14.202 ± 0.018	14.202 ± 0.018	-1.808 ± 0.102
	1611	< 14.785		
NiII	1370	12.920 ± 0.103	12.900 ± 0.042	-1.850 ± 0.108
	1703	< 13.575		
	1709	12.871 ± 0.088		
	1741	12.990 ± 0.064		
	1751	12.817 ± 0.090		
ZnII	2026	11.496 ± 0.103	11.496 ± 0.103	-1.654 ± 0.144
	2062	< 11.697		

The damped Ly α system toward Q0347-38 is another member of the LBQS statistical sample, one of the four with $z_{abs} > 3$. We adopt $\log N({\rm HI}) = 20.8 \pm 0.1$ based on a measurement by Pettini et al. (1994). This is one of the few systems where we have an estimate of $N(S^+)$, although we note SII 1259 is partially blended with the ${\rm Ly}\alpha$ forest and should be considered an upper limit to the true S abundance, $N(S^+) < 10^{14.73} \,\mathrm{cm}^{-2}$. We discuss the S/Fe ratio in detail below, noting here that the value has particular impact on interpreting the abundances of the damped $Lv\alpha$ systems with respect to Type II SN enrichment and dust depletion. The system is also notable for the easily identifiable excited fine structure CII* 1335 transition. Unfortunately, the CII 1334 profile is so heavily saturated that no meaningful comparison can be made with the fine structure transition. Finally, we observe a very low Ni abundance for this system, [Ni/H] < -2.37 dex, implying [Ni/Fe] < -0.5 dex which may be difficult to explain within the leading explanations for the damped Ly α abundance patterns.

3.6.
$$Q0458-02$$
, $z=2.040$

This damped Ly α system is 'famous' for exhibiting HI 21cm absorption. In particular, Briggs et al. (1989) have used VLBI radio observations to place a lower limit on its size of 8 h_{100}^{-1} kpc. In our analysis we adopt $\log N(\mathrm{HI}) = 21.65 \pm 0.09$ taken from Pettini et al. (1994). A plot of the metal-line profiles is given in Figure 6 and Table 8 lists the column densities. Note the CII* 1335 profile is heavily saturated. Assuming the $^2P_{3/2}$ excited fine-structure state is populated by e⁻ collisions and $N(\mathrm{C}^+) < 10^{17}\,\mathrm{cm}^{-2}$ (which follows by assuming [C/H] < [Zn/H]), the limit on $N(\mathrm{CII}^*)$ indicates $n_e > 0.1\,\mathrm{cm}^{-3}$. The system, with one of the highest measured $N(\mathrm{HI})$ values, must have a high neu-

 $\label{eq:table 7} \text{Table 7}$ Ionic Column Densities: Q0347—38, z=3.025

		35. €0011 00, ≈	
λ	AODM	N_{adopt}	[X/H]
1215	20.800 ± 0.100		
1334	> 15.027	> 15.027	> -2.333
1335	13.477 ± 0.032		
1548	13.846 ± 0.011		
1550	13.783 ± 0.020		
1302	> 15.379	< 17.740	< 0.010
1355	< 17.740		
1260	> 14.268	14.820 ± 0.028	-1.530 ± 0.104
1304	14.820 ± 0.028		
1526	> 14.748		
1393	13.750 ± 0.017		
1259	14.731 ± 0.012	14.731 ± 0.012	-1.339 ± 0.101
1608	14.472 ± 0.007	14.472 ± 0.007	-1.838 ± 0.100
1611	< 14.476		
1370	< 12.677	< 12.677	< -2.373
	1215 1334 1335 1548 1550 1302 1355 1260 1304 1526 1393 1259 1608 1611	$\begin{array}{cccc} 1215 & 20.800 \pm 0.100 \\ 1334 & > 15.027 \\ 1335 & 13.477 \pm 0.032 \\ 1548 & 13.846 \pm 0.011 \\ 1550 & 13.783 \pm 0.020 \\ 1302 & > 15.379 \\ 1355 & < 17.740 \\ 1260 & > 14.268 \\ 1304 & 14.820 \pm 0.028 \\ 1526 & > 14.748 \\ 1393 & 13.750 \pm 0.017 \\ 1259 & 14.731 \pm 0.012 \\ 1608 & 14.472 \pm 0.007 \\ 1611 & < 14.476 \\ \end{array}$	$\begin{array}{cccccccccccccccccccccccccccccccccccc$

tral fraction implying $n_H > 0.1 \, \mathrm{cm}^{-3}$. Because FeII 1608 is saturated, we base the Fe abundance on the FeII 1611 transition. Finally, we note the ZnII 2026 profile is blended with an unidentified line at $v > 20 \, \mathrm{km \ s^{-1}}$ and therefore the AODM was applied only to $v = +20 \, \mathrm{km \ s^{-1}}$.

 $\label{eq:table 8} \text{Ionic Column Densities: } Q0458-02,\,z=3.040$

		COLUMN BENSITIE	z. v €0100 0=, ≈	- 0.040
Ion	λ	AODM	N_{adopt}	[X/H]
HI	1215	21.650 ± 0.090		
CII	1334	> 15.010		
	1335	> 14.794		
CIV	1548	> 14.906		
	1550	> 15.111		
OI	1302	> 15.410		
	1355	< 18.560		
AlII	1670	> 13.720		
AlIII	1854	13.334 ± 0.018		
	1862	13.335 ± 0.022		
SiII	1304	> 15.095	> 15.095	> -2.105
	1526	> 14.981		
	1808	> 16.021		
SiIV	1393	> 14.262		
	1402	> 14.481		
CrII	2056	13.756 ± 0.013	13.797 ± 0.008	-1.533 ± 0.090
	2062	13.763 ± 0.014		
	2066	13.987 ± 0.015		
FeII	1608	> 15.136	15.508 ± 0.048	-1.652 ± 0.102
	1611	15.508 ± 0.048		
NiII	1317	13.985 ± 0.024	13.853 ± 0.019	-2.047 ± 0.092
	1709	13.840 ± 0.035		
	1741	13.936 ± 0.032		
	1751	13.808 ± 0.033		
ZnII	2026	13.141 ± 0.018	13.141 ± 0.018	-1.159 ± 0.092

3.7. Q0841+12, $z = 2.375 \ \& \ z = 2.476$

The damped Ly α systems toward this BL Lac object were first identified by C. Hazard and were subsequently analyzed by Pettini et al. (1997). We take $N({\rm HI})=20.95\pm0.087$ for the system at z=2.375 and $N({\rm HI})=20.78\pm0.097$ for the system at z=2.476 (Pettini et al. 1997). Figures 7 and 8 plot the metal-line profiles for these systems and Tables 9 and 10 list the ionic column densities. The profiles for the lower redshift system have good SNR and the derived column densities are accurate.

Unfortunately, its FeII 1608 and FeII 1611 transitions are blended with sky lines. In the abundance analysis, then, we will adopt an Fe abundance, [Fe/H] = [Cr/H], motivated by the fact that [Cr/Fe] ≈ 0 in the damped systems. For the system at z=2.476, SiII 1808 is blended with the AlIII 1862 transition from the z=2.375 system and also may be contaminated by a sky line. Therefore, we adopt a lower limit to $N(\mathrm{Si}^+)$ from the saturated SiII 1526 profile. Finally, we obtain an upper limit measurement for $N(\mathrm{Zn}^+)$ for this system which is a significant improvement over previous efforts (Pettini et al. 1997).

7

 $\label{eq:table 9} \text{Ionic Column Densities: } Q0841+12,\,z=2.375$

		0 0 0 0 0 0 0 0 0 0 0 0 0 0 0 0 0 0 0 0	5. % 0011 12, ≈	=.0,0
Ion	λ	AODM	N_{adopt}	[X/H]
HI	1215	20.950 ± 0.087		
CIV	1548	13.968 ± 0.011		
	1550	13.973 ± 0.015		
AlII	1670	> 13.267	> 13.267	> -2.163
AlIII	1854	12.504 ± 0.029		
	1862	12.703 ± 0.035		
SiII	1526	> 14.566	15.239 ± 0.024	-1.261 ± 0.090
	1808	15.239 ± 0.024		
CrII	2056	12.960 ± 0.061	13.079 ± 0.027	-1.551 ± 0.091
	2062	13.185 ± 0.034		
	2066	13.035 ± 0.059		
NiII	1454	13.211 ± 0.075	13.243 ± 0.030	-1.957 ± 0.092
	1741	13.297 ± 0.039		
	1751	13.185 ± 0.055		
$_{ m ZnII}$	2026	12.114 ± 0.057	12.115 ± 0.049	-1.485 ± 0.100
	2062	12.115 ± 0.099		

 $\label{eq:table 10} \text{Table 10}$ Ionic Column Densities: Q0841+12, z=2.476

	IONIC (COLUMN DENSITIE	S: $Q0841+12, z =$	= 2.476
Ion	λ	AODM	N_{adopt}	[X/H]
$_{ m HI}$	1215	20.780 ± 0.097		
CIV	1548	13.914 ± 0.009		
	1550	13.986 ± 0.012		
AlII	1670	13.186 ± 0.286	13.186 ± 0.286	-2.074 ± 0.302
AlIII	1854	12.683 ± 0.027		
	1862	12.633 ± 0.038		
SiII	1526	> 14.461	> 14.461	> -1.869
	1808	14.958 ± 0.022		
SiIV	1393	13.646 ± 0.009		
	1402	13.646 ± 0.011		
TiII	1910	< 12.434	< 12.434	< -1.276
CrII	2056	12.907 ± 0.043	12.840 ± 0.036	-1.620 ± 0.103
	2062	12.759 ± 0.061		
	2066	< 12.802		
FeII	1608	14.434 ± 0.027	14.434 ± 0.027	-1.856 ± 0.101
	1611	< 14.668		
NiII	1741	13.067 ± 0.052	13.048 ± 0.049	-1.982 ± 0.108
	1751	12.965 ± 0.129		
$_{ m ZnII}$	2026	< 11.778	< 11.778	< -1.652
	2062	< 11.772		

3.8. Q0951-04, z = 3.857 & z = 4.203

The QSO Q0951–04 from the survey by Storrie-Lombardi et al. (1996) has two intervening damped Ly α systems, both at very high redshift. The velocity plots and measurements for the z=3.857 system are given in Figure 9 and Table 11, while those for the z=4.203 system are presented by Figure 10 and Table 12. We adopt

 $\log N({
m HI}) = 20.6 \pm 0.1$ for the system at z=3.857 and $\log N({
m HI}) = 20.4 \pm 0.1$ for the system at z=4.203, based on recent Keck measurements (Storrie-Lombardi and Wolfe 1998). Because all of the column densities are based on either marginally saturated profiles or weaker, low SNR profiles all of these measurements are somewhat tentative. In fact, we consider the limits on $N({
m Fe}^+)$ for the system at z=4.203 to be too conservative to include this system in the abundance analysis. Finally, we note the feature at $v=180~{\rm km~s}^{-1}$ in the NiII 1370 profile for the z=3.857 system may be an unidentified blend, although it nearly coincides with a strong feature in the SiII 1526 profile.

 $\label{eq:table 11} \text{Ionic Column Densities: Q0951-04, } z = 3.857$

Ion	λ	AODM	N_{adopt}	[X/H]
HI	1215	20.600 ± 0.100		
AlII	1670	13.298 ± 0.022	13.298 ± 0.022	-1.782 ± 0.102
SiII	1526	14.645 ± 0.030	14.645 ± 0.030	-1.505 ± 0.104
SiIV	1393	13.900 ± 0.011		
FeII	1608	14.062 ± 0.060	14.062 ± 0.060	-2.048 ± 0.117
NiII	1370	12.994 ± 0.099	12.994 ± 0.099	-1.856 ± 0.141

 $\label{eq:table 12} \text{Ionic Column Densities: } Q0951-04,\,z=4.203$

Ion	λ	AODM	N_{adopt}	[X/H]
HI	1215	20.400 ± 0.100		
OI	1302	14.607 ± 0.323	14.607 ± 0.323	-2.723 ± 0.339
SiII	1190	13.455 ± 0.050	13.392 ± 0.032	-2.558 ± 0.105
	1304	13.286 ± 0.060		
	1526	13.483 ± 0.055		
FeII	1608	< 13.281	< 13.281	< -2.629
	1611	< 15.153		
NiII	1317	< 12.589	< 12.589	< -2.061
	1370	< 12.625		

3.9.
$$Q1215+33$$
, $z=1.999$

This radio-selected damped system (Wolfe et al. 1986) was observed as part of the commissioning run for the HIRES instrument and is a member of the LBQS statistical sample. In the following analysis we assume $\log N({\rm HI}) = 20.95 \pm 0.067$ based on observations by Pettini et al. (1994). Figure 11 presents a plot of the metalline transitions and the ionic column densities are listed in Table 13. As the FeII 1608 profile is saturated and the FeII 1611 transition is marginally detected, we establish only a lower limit to $N({\rm Fe^+})$. We will include this system in the abundance analysis, however, by adopting $\log 10[N({\rm Fe^+})] = 14.648 \pm 0.033$ based solely on the FeII 1608 profile, noting this value may be an underestimate.

3.10.
$$Q1331+17$$
, $z=1.776$

This famous damped Ly α system which exhibits 21cm absorption (Wolfe & Davis 1979) has been studied by a number of authors (over 100 papers), yet never with the quality of data presented here (FWHM resolution

 $\label{eq:Table 13} \text{Ionic Column Densities: Q1215+33, } z = 1.999$

Ion	λ	AODM	N_{adopt}	[X/H]
$_{ m HI}$	1215	20.950 ± 0.067		
CIV	1548	13.605 ± 0.019		
	1550	13.672 ± 0.030		
OI	1355	< 17.952	< 17.952	< 0.072
AlII	1670	> 13.358		
AlIII	1854	12.746 ± 0.017		
	1862	12.783 ± 0.021		
SiII	1526	> 14.681	15.030 ± 0.025	-1.470 ± 0.072
	1808	15.030 ± 0.025		
SiIV	1393	12.993 ± 0.039		
CrII	2056	13.173 ± 0.034	13.130 ± 0.031	-1.500 ± 0.074
	2062	13.034 ± 0.066		
FeII	1608	14.648 ± 0.039	14.648 ± 0.039	-1.812 ± 0.078
	1611	14.925 ± 0.100		
NiII	1741	13.419 ± 0.040	13.344 ± 0.033	-1.856 ± 0.075
	1751	13.262 ± 0.056		
ZnII	2026	12.291 ± 0.058	12.291 ± 0.058	-1.309 ± 0.089

 $\approx 6 \text{ km s}^{-1} \text{ and SNR} > 50$). Table 14 lists the column densities for the metal-line transitions and Figure 12 plots their profiles. We assume $\log N({\rm HI}) = 21.176 \pm 0.041$ (Pettini et al. 1994). The SNR is excellent throughout the entire spectrum yielding very accurate column density measurements. This is one of the very few systems where CI absorption is detected and Songaila et al. (1994) have used measurements of the CI profile to estimate the cosmic background temperature at z = 1.776. Consider the feature at $v = +20 \text{ km s}^{-1}$ which is fully resolved in the CI profiles, barely resolved in the Zn⁺ profiles, and is unresolved in the stronger transitions even at 6 km $\rm s^{-1}$ resolution. This suggest the gas in this component is at a temperature T < 6000K. While this system may be atypical because it is one of the few damped systems to exhibit CI absorption, it is worth noting a majority of observed damped Ly α profiles may be the result of the superposition of many narrow components.

 $\label{eq:Table 14} \text{Ionic Column Densities: Q1331+17, } z = 1.776$

Ion	λ	AODM	N_{adopt}	[X/H]
HI	1215	21.176 ± 0.041	,	
CI	1560	13.573 ± 0.013		
	1656	13.312 ± 0.012		
CIV	1548	> 15.073		
	1550	> 15.172		
AlII	1670	> 13.573		
AlIII	1854	13.004 ± 0.004		
	1862	12.968 ± 0.007		
SiII	1526	> 14.951	15.285 ± 0.004	-1.441 ± 0.041
	1808	15.285 ± 0.004		
CrII	2056	12.950 ± 0.017	12.919 ± 0.015	-1.937 ± 0.044
	2066	12.834 ± 0.034		
FeII	1608	14.601 ± 0.003	14.598 ± 0.001	-2.088 ± 0.041
	2344	14.597 ± 0.022		
	2374	14.598 ± 0.002		
	2382	> 14.433		
NiII	1709	13.166 ± 0.017	13.235 ± 0.009	-2.191 ± 0.042
	1741	13.313 ± 0.011		
	1751	13.165 ± 0.022		
ZnII	2026	12.605 ± 0.009	12.605 ± 0.008	-1.221 ± 0.042
	2062	12.605 ± 0.013		

3.11. Q1346-03, z = 3.736

This very high z damped Ly α system was taken from the survey of Storrie-Lombardi et al. (1996). We present the velocity plots and column densities in Figure 13 and Table 15. We adopt $\log N({\rm HI}) = 20.7 \pm 0.1$ (Storrie-Lombardi and Wolfe 1998) throughout the analysis. Unfortunately both FeII 1608 and FeII 1611 are blended with B-band sky lines. Therefore, we have no metallicity indicator for this system and it is not included in the subsequent analysis. Measuring [Si/H] = -2.3 dex, we expect this is a very metal-poor system.

 $\label{eq:table 15} \text{Ionic Column Densities: Q1346-03, } z = 3.736$

		COLUMN BENGITH	EB. Q 1010 00, ≈	
Ion	λ	AODM	N_{adopt}	[X/H]
HI	1215	20.700 ± 0.100		
CII	1334	14.422 ± 0.095	14.422 ± 0.095	-2.838 ± 0.138
AlII	1670	12.546 ± 0.025	12.546 ± 0.025	-2.634 ± 0.103
SiII	1304	13.961 ± 0.012	13.954 ± 0.011	-2.296 ± 0.101
	1526	13.923 ± 0.026		
SiIV	1393	12.344 ± 0.096		
	1402	< 12.598		
NiII	1370	< 12.694		
	1741	< 13.024		

3.12. Q1759+75, z=2.625

This system and the adopted $N({\rm HI})=20.8\pm0.1$ are taken from an ongoing survey by I. Hook. Figure 14 presents the velocity plots and Table 16 gives the measurements. The QSO is very bright and was observed at FWHM $\approx 6~{\rm km~s^{-1}}$ resolution. We expect all of the measured abundances are very accurate with the exception of $N({\rm Zn^+})$ where the ZnII 2026 profile is blended with sky lines. Although the strongest feature appears unblended, we have chosen not to include Zn in the abundance analysis.

 $\label{eq:table 16} \text{Ionic Column Densities: Q1759+75, } z = 2.625$

	101110	COLUMN DENSITIE	B. €21100 10, ≈	_ 2.020
Ion	λ	AODM	N_{adopt}	[X/H]
HI	1215	20.800 ± 0.100		
CIV	1548	14.636 ± 0.019		
	1550	14.647 ± 0.005		
AlIII	1854	13.623 ± 0.004		
SiII	1526	> 15.014	15.532 ± 0.008	-0.818 ± 0.100
	1808	15.532 ± 0.008		
CrII	2066	13.211 ± 0.062	13.211 ± 0.062	-1.269 ± 0.117
FeII	1608	> 14.980	15.076 ± 0.042	-1.234 ± 0.108
	1611	15.076 ± 0.042		
NiII	1454	13.589 ± 0.039	13.565 ± 0.011	-1.485 ± 0.101
	1709	13.615 ± 0.020		
	1741	13.582 ± 0.017		
	1751	13.506 ± 0.021		
ZnII	2026	> 11.650	> 11.650	> -1.800

3.13. Q2230+02, z = 1.864

Figure 15 presents the velocity plots for the damped Ly α system toward Q2230+02 and Table 17 lists the measured ionic column densities. We adopt $\log N({\rm HI}) =$

 20.85 ± 0.084 (Pettini et al. 1994) for this LBOS damped system. We have wavelength coverage of 28 metal-line transitions and have determined accurate column densities for the majority of them. This system is notable for a 4σ detection of $N(\text{Ti}^+)$. There are two TiII transitions at 1910 Awith similar oscillator strengths and the profiles cannot be disentangled. Following the analysis presented in Prochaska & Wolfe (1997a), we integrate N_a over the entire velocity region associated with the TiII transitions and use a reduced oscillator strength, $f^* \equiv (f_1^2 + f_2^2)/(f_1 + f_2) = 0.0862$, to calculate $N(\text{Ti}^+)$. There is another difficulty in determining the Ti⁺ column density for this system. An emission line feature lies just blueward of the TiII profiles and causes problems in determining the continuum level. This leads to a systematic error estimated at 0.1 dex.

The profile for the low-ion transitions is comprised of three primary features whose relative optical depth apparently varies from transition to transition. For instance, the central feature is the strongest in the SiII 1808, CrII 2062, CrII 2066, and ZnII 2026 profiles and the weakest in the FeII 2260 and CrII 2056 transitions. While differences in the level of dust depletion could account for some of the variations, it would be impossible to explain the differences for a single ion (e.g. the CrII transitions). The most likely explanation is that this central feature is a very narrow component – not fully resolved at our resolution – whose relative optical depth varies significantly with the strength of the transition. Finally, this system is notable for the presence of a nearby metal-line system at $\approx -550 \, \mathrm{km \ s^{-1}}$ which shows multiple metal transitions (Figure 16). The subsystem exhibits ionic column densities typical of a damped Ly α system and its $Al^{+}/Al^{++} = 2.6$ ratio indicates the system is nearly neutral. Therefore, it is almost certainly contributing to the measured $N(\mathrm{HI})$ for this system which would mean we are underestimating the metallicity of the system at z = 1.864. Because the nearby system exhibits ionic column densities at < 10% of the damped system, we have chosen to ignore its effects in our abundance analysis.

3.14.
$$Q2231-00$$
, $z=2.066$

This LBQS system is another damped Ly α system exhibiting significant (5σ) TiII 1910 absorption. As in the damped Ly α system toward Q2230+02, the TiII profiles overlap, hence we use the technique outlined above to determine $N(\mathrm{Ti}^+)$. Throughout the analysis we adopt $\log N(\mathrm{HI}) = 20.56 \pm 0.1$ (Pettini et al. 1994). The velocity plots are given in Figure 17 and the column densities are presented in Table 18. This is the other system in our data sample which was previously observed by Lu et al. (1996). We find our measurements match theirs in nearly every case, although their analysis did not include Ti⁺.

3.15.
$$Q2348-14$$
, $z=2.279$

This very metal-poor system was first discussed by Pettini et al. (1994) and has been previously observed at high resolution by Pettini et al. (1995). In Figure 19 we plot the Ly α transition for this system. Overplotted are Voigt profiles centered at z=2.2794 with $\log N({\rm HI})=20.56\pm0.075$ corresponding to the measurements made by Pettini et al. (1994). While the profiles provide a reasonable fit to the

 $\label{eq:table 17} \text{Ionic Column Densities: Q2230+02, } z = 1.864$

Ion	λ	AODM	N_{adopt}	[X/H]
HI	1215	20.850 ± 0.084		
CIV	1548	> 14.848		
	1550	14.808 ± 0.007		
AlII	1670	> 14.020		
AlIII	1854	13.590 ± 0.006		
	1862	13.596 ± 0.009		
SiII	1526	> 15.233	15.656 ± 0.010	-0.744 ± 0.085
	1808	15.656 ± 0.010		
SiIV	1393	> 14.267		
	1402	> 14.354		
TiII	1910	12.985 ± 0.099	12.985 ± 0.099	-0.795 ± 0.130
CrII	2056	13.361 ± 0.036	13.403 ± 0.027	-1.127 ± 0.088
	2066	13.483 ± 0.041		
FeII	1608	> 15.115	15.188 ± 0.016	-1.172 ± 0.086
	1611	15.273 ± 0.084		
	2249	15.120 ± 0.036		
	2260	15.210 ± 0.019		
	2344	> 14.988		
	2374	> 15.183		
	2382	> 14.723		
NiII	1370	13.883 ± 0.052	13.812 ± 0.011	-1.288 ± 0.085
	1709	13.860 ± 0.014		
	1741	13.838 ± 0.023		
	1751	13.687 ± 0.028		
ZnII	2026	12.800 ± 0.028	12.800 ± 0.028	-0.700 ± 0.088

 $\label{eq:table 18} \text{Ionic Column Densities: Q2231-00, } z = 2.066$

Ion	λ	AODM	N_{adopt}	[X/H]
HI	1215	20.560 ± 0.100		
CII	1335	13.580 ± 0.040		
CIV	1548	14.195 ± 0.005		
OI	1302	> 15.543	< 17.748	< 0.258
	1355	< 17.748		
AlIII	1854	13.172 ± 0.010		
	1862	13.110 ± 0.023		
SiII	1304	> 15.030	15.247 ± 0.019	-0.863 ± 0.102
	1526	> 15.014		
	1808	15.247 ± 0.019		
SiIV	1393	13.704 ± 0.010		
	1402	13.698 ± 0.012		
TiII	1910	12.848 ± 0.071	12.848 ± 0.071	-0.642 ± 0.123
CrII	2062	13.182 ± 0.040	13.165 ± 0.034	-1.075 ± 0.106
	2066	13.130 ± 0.063		
FeII	1608	14.750 ± 0.009	14.750 ± 0.009	-1.320 ± 0.100
	1611	14.783 ± 0.065		
NiII	1370	12.880 ± 0.091	13.306 ± 0.032	-1.504 ± 0.105
	1741	13.381 ± 0.033		
	1751	13.100 ± 0.091		
ZnII	2026	12.463 ± 0.023	12.463 ± 0.023	-0.747 ± 0.103

left wing of the damped profile, the fit for $v > 750~\rm km~s^{-1}$ is clearly inconsistent for all of the assumed $N(\rm HI)$ values. It is very difficult, however, to continuum fit an order of HIRES data which includes a damped Ly α profile; it is easier to fit intermediate resolution data. Therefore, we adopt $\log N(\rm HI) = 20.56 \pm 0.075$ from the Pettini et al. analysis, but note in passing that this may be an overestimate of the true $N(\rm HI)$ value. Comparing our derived chemical abundances with the work of Pettini et al. (1995) we find reasonable agreement and note we have improved on their limits in a few cases (e.g. N and S).

The system is exceptional for a number of reasons. First,

it is one of the few systems where we have a measurement of $N(S^+)$ based on the SII 1259 transition. As discussed for the damped system toward Q0347-38, S/Fe is an excellent diagnostic of dust depletion. Here we find [S/Fe] = 0.17 dex which argues strongly against dust depletion if the system has an underlying Type II SN pattern. Second, the system exhibits two distinct low-ion features, one at $v \approx -100 \,\mathrm{km} \,\mathrm{s}^{-1}$ (feature 1; this feature was not resolved in previous observations) and the more dominant at $v \approx 0 \text{ km s}^{-1}$ (feature 2). Feature 1 is present in all of the SiII transitions and is the strongest feature in the AlIII, CIV and SiIV profiles. Comparing $N(Si^+)$ for the two features in the SiII 1526 profile, we find $N(\mathrm{Si}^+)_1/N(\mathrm{Si}^+)_2 = 0.18$. At the same time, however, the feature is entirely absent in the OI 1302 and FeII 1608 profiles: $N({\rm O^0})_1/N({\rm O^0})_2 < 0.027$ and $N(\text{Fe}^+)_1/N(\text{Fe}^+)_2 < 0.07$. While dust could possibly explain the absence of Fe where Si is present because Si is only lightly depleted in the ISM, it cannot account for the lack of OI absorption. The system corresponding to feature 1 must be significantly ionized such that the dominant states of O, Fe, and Si are higher ions. We have performed CLOUDY (Ferland 1991) calculations which demonstrate values of $[\mathrm{Si}^+/\mathrm{O}^0] \approx 1.2$ dex and $[\mathrm{Si}^+/\mathrm{Fe}^+] \approx 0.7$ dex are possible in a Lyman limit system provided the ionization parameter is significantly high. Therefore, we argue feature 2 marks the damped Ly α system while feature 1 may be a significantly ionized satellite or halo cloud. The system is also notable for providing a meaningful estimate of N/O. Finally, perhaps the most remarkable characteristic of this damped system is the velocity width of the CIV profiles, $\Delta v > 600 \text{ km s}^{-1}$, particularly in light of the very narrow Δv exhibited by the low-ion profiles. This kinematic observation poses a difficult challenge to any physical model introduced to explain the damped Ly α systems.

 $\label{eq:table 19} \text{Ionic Column Densities: } \text{Q2348-14, } z = 2.279$

	TONIC	COLUMN DENSITIE	5. Q2546-14, z	= 2.219
Ion	λ	AODM	N_{adopt}	[X/H]
$_{ m HI}$	1215	20.560 ± 0.075		
CII	1334	> 14.610		
	1335	13.207 ± 0.070		
NI	1200	< 13.223	< 13.223	< -3.387
OI	1302	> 14.798	> 14.798	> -2.692
AlII	1670	12.654 ± 0.006	12.654 ± 0.006	-2.386 ± 0.075
AlIII	1854	12.726 ± 0.012		
	1862	12.613 ± 0.027		
SiII	1190	> 14.207	14.201 ± 0.010	-1.909 ± 0.076
	1193	> 13.924		
	1260	> 13.744		
	1304	14.227 ± 0.021		
	1526	14.201 ± 0.011		
	1808	14.089 ± 0.059		
SiIV	1393	> 14.063		
SII	1259	13.725 ± 0.119	13.725 ± 0.119	-2.105 ± 0.140
FeII	1608	13.792 ± 0.016	13.792 ± 0.016	-2.278 ± 0.077

3.16. Q2359-02, z=2.095 & z=2.154

This faint QSO exhibits two intervening damped Ly α systems. Both are members of the LBQS statistical survey. The velocity plots and column densities for the z=2.095 system are presented in Figure 20 and Table 20 and those

for the z=2.154 are given by Figure 21 and Table 21. Both are part of the LBQS statistical sample and we have taken the HI column densities from Wolfe et al. (1995): $\log N({\rm HI}) = 20.7 \pm 0.1$ for the z=2.095 system and $\log N({\rm HI}) = 20.3 \pm 0.1$ for the z=2.154 system. The SNR is relatively low for most of the spectrum and therefore abundances established on the weakest transitions are suspect, particularly those for Zn. We intend to make further observations of these two systems to improve the accuracy of our abundance measurements.

Table 20

	IONIC (Column Densitie	s: $Q2359-02, z =$	= 2.095
Ion	λ	AODM	N_{adopt}	[X/H]
HI	1215	20.700 ± 0.100		
CII	1334	> 15.146		
CIV	1548	> 14.639		
	1550	> 14.800		
AlII	1670	13.662 ± 0.034	13.662 ± 0.034	-1.518 ± 0.106
AlIII	1854	13.383 ± 0.010		
	1862	13.396 ± 0.016		
SiII	1526	> 15.045	15.408 ± 0.021	-0.842 ± 0.102
	1808	15.408 ± 0.021		
SiIV	1393	> 14.072		
	1402	> 14.517		
CrII	2056	12.748 ± 0.091	12.748 ± 0.091	-1.632 ± 0.135
	2062	13.131 ± 0.057		
	2066	< 12.897		
FeII	1608	14.507 ± 0.025	14.507 ± 0.025	-1.703 ± 0.103
	1611	< 15.077		
NiII	1703	< 13.693	13.142 ± 0.054	-1.808 ± 0.114
	1709	13.152 ± 0.127		
	1741	13.185 ± 0.072		
	1751	13.071 ± 0.107		
ZnII	2026	12.595 ± 0.029	12.595 ± 0.029	-0.755 ± 0.104
	2062	12.486 ± 0.075		

 $\label{eq:table 21} \text{Ionic Column Densities: Q2359-02, } z = 2.154$

			•	
Ion	λ	AODM	N_{adopt}	[X/H]
HI	1215	20.300 ± 0.100		
CII	1334	> 14.987		
CIV	1548	> 14.880		
	1550	> 14.966		
AlII	1670	13.165 ± 0.016	13.165 ± 0.016	-1.615 ± 0.101
AlIII	1862	12.960 ± 0.021		
SiII	1526	14.316 ± 0.015	14.316 ± 0.015	-1.534 ± 0.101
SiIV	1393	> 14.568		
	1402	> 14.528		
CrII	2056	< 12.549	< 12.946	< -1.034
	2066	< 12.946		
FeII	1608	13.895 ± 0.032	13.895 ± 0.032	-1.915 ± 0.105
	1611	< 14.917		
NiII	1317	< 13.152	< 12.949	< -1.601
	1370	< 13.248		
	1454	< 13.063		
	1741	< 12.949		
	1751	< 13.200		
ZnII	2026	< 11.901	< 11.901	< -1.049

4. ABUNDANCE PATTERNS

Table 22 lists the relative logarithmic abundances for the damped Ly α systems, [X/H] $\equiv \log[N(X)/N(H)] - \log[N(X)/N(H)]_{\odot}$. For each system we adopt the value

ı																							I
	Q2359-02B	Q2359-02A	Q2348-14	Q2231-00	Q2230+02	Q2206-19B	Q2206-19A	Q1759+75	Q1346-03	Q1331+17	Q1215+33	Q0951 - 04B	Q0951 - 04A	Q0841 + 12B	Q0841 + 12A	Q0458 - 02	Q0347 - 38	Q0201 + 36	Q0149 + 33	Q0100+13	Q0019-01	Q0000-26	DLA
	2.154	2.095	2.279	2.066	1.864	2.076	1.920	2.625	3.736	1.776	1.999	4.203	3.857	2.476	2.375	2.040	3.025	2.463	2.141	2.309	3.439	3.390	z_{abs}
	20.300	20.700	20.560	20.560	20.850	20.431	20.653	20.800	20.700	21.176	20.950	20.400	20.600	20.780	20.950	21.650	20.800	20.380	20.500	21.400	20.900	21.410	$\log[N(HI)]$
	-1.534	-0.842	-1.909	-0.863	-0.744	-2.225	-0.402	-0.818	-2.296	-1.441	-1.470	-2.558	-1.505	> -1.869	-1.261	> -2.105	-1.530	-0.376	-1.683	> -2.228	-1.027	-1.874	[S1/H]
	-1.615	-1.518	-2.386			-2.727			-2.634				-1.782	-2.074	> -2.163				-2.044				[AI/H]
			-2.105														-1.339						[D/H]
	-1.915	-1.703	-2.278	-1.320	-1.172	-2.621	-0.705	-1.234		-2.088	-1.812	< -2.629	-2.048	-1.856	-2.015	-1.652	-1.838	-0.878	-1.808	-1.814	-1.640	-1.774	[Fe/H]
	< -1.601	-1.808		-1.504	-1.288		-0.903	-1.485		-2.191	-1.856	< -2.061	-1.856	-1.982	-1.957	-2.047	< -2.373	-0.877	-1.850	-2.030	-1.708	-2.335	[N1/H]
	< -1.034	-1.632		-1.075	-1.127		-0.580	-1.269		-1.937	-1.500			-1.620	-1.551	-1.533		-0.776	-1.369	-1.693			[Cr/H]
	< -1.04	-0.755		-0.747	-0.700		-0.379	> -1.80		-1.221	-1.309			< -1.65	-1.485	-1.159		-0.266	-1.654	-1.556			[Zn/H]

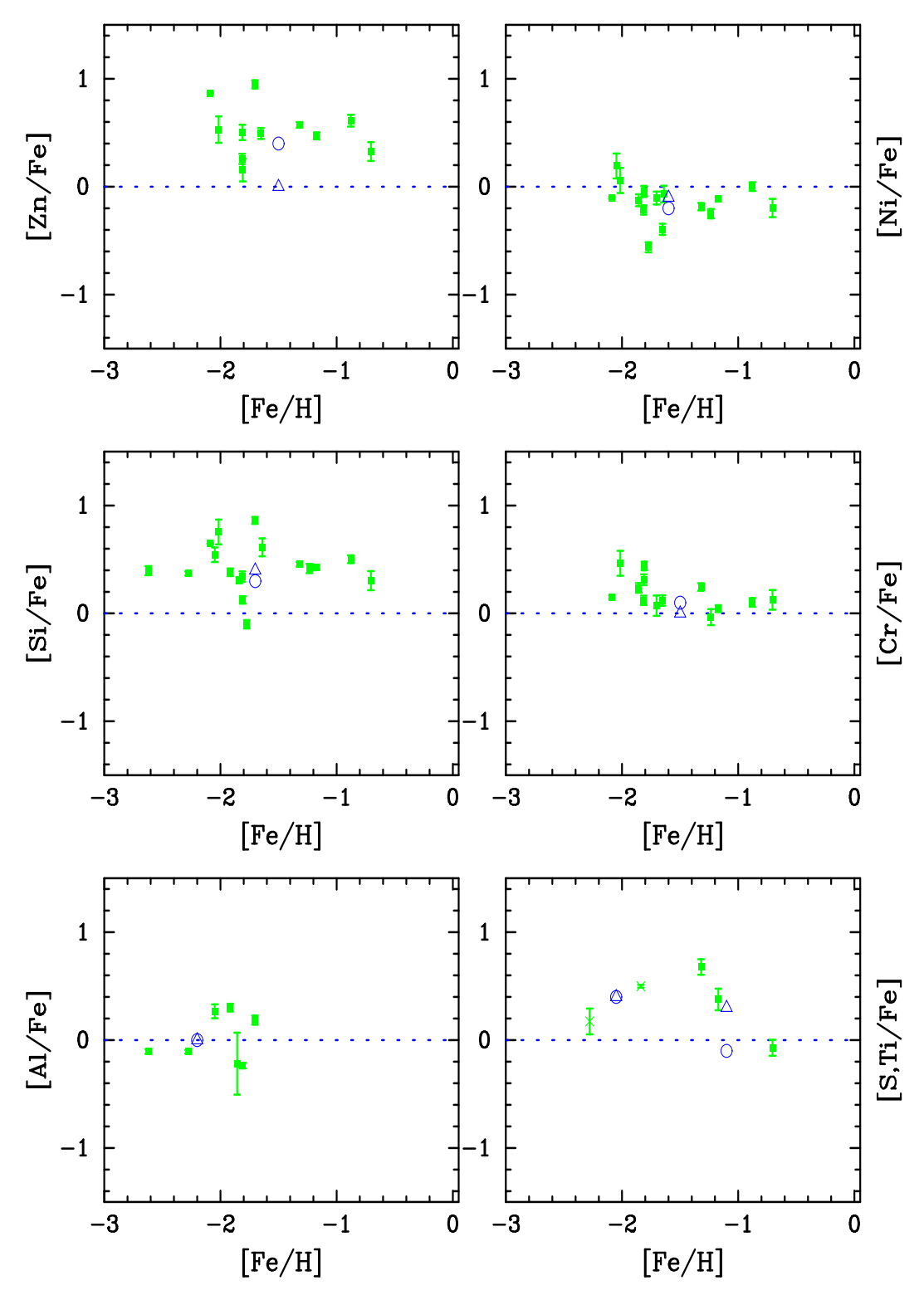


Fig. 22.— Abundance patterns of the most common elements from our full damped Ly α sample. Following standard practice in stellar abundance analysis we plot [X/Fe], the logarithmic abundance of element X to Fe relative to solar. We plot this quantity vs. [Fe/H], an indicator of the metallicity of the system. The triangles printed in each panel represent the typical metal-poor halo value (McWilliam 1997). The circles indicate the observed pattern for lightly depleted ISM gas (Savage and Sembach 1996). In the lower right panel, the x's identify [S/Fe] values and the squares mark [Ti/Fe].

for $N({\rm HI})$ indicated in the previous section, and calculate $N({\rm X})$ by performing a weighted mean of all direct measurements, i.e. no limits or blends. Included in Table 22 are the abundance measurements for the damped Ly α systems toward Q0201+36 and Q2206-19. In a few cases the values differ from the published values in light of new oscillator strengths. It is well-established both observationally and theoretically that the damped Ly α systems are primarily neutral (Viegas 1994, Prochaska & Wolfe 1996). Therefore we perform no ionization corrections in determining the abundances from the ionic column densities of the low-ions.

Figure 22 presents the abundance patterns for the most common elements in our full sample. We have chosen not to include error bars for presentation purposes; the derived errors are < 0.1 dex with only a few exceptions. Following Lu et al. (1996), along the x-axis of each panel we plot metallicity – here expressed with [Fe/H] – in part because this is the primary metallicity indicator in local stellar populations and in part because we have Fe abundance measurements for a greater number of systems. Examining the upper-left panel of Figure 22, we note a systematic overabundance of Zn/Fe which suggests Fe may be depleted onto dust grains. Therefore consider the [Fe/H] values to be lower limits to the true metallicity. In one case where (Q0841+12A) we have no reliable Fe abundance measurement and have taken [Fe/H] = [Cr/H] on the grounds that $[Cr/H] \approx [Fe/H]$ in the majority of damped Ly α systems.

In the following, we discuss the evidence for dust depletion and Type II supernovae enrichment in light of the observed damped Ly α abundance patterns. The former is determined by comparing against abundance patterns in depleted ISM clouds (Savage and Sembach 1996) while the latter is assessed by comparing against the abundance patterns of metal-poor halo stars presumed to exhibit nucleosynthetic patterns typical of Type II supernovae (McWilliam 1997). First, consider the top two panels of Figure 22 which lend support to the presence of significant dust depletion in the damped Ly α systems. As described throughout the paper, the overabundance of Zn to Fe relative to solar abundances is suggestive of dust depletion both because (i) Zn is largely undepleted in dusty regions within the ISM whereas Fe is heavily depleted and (ii) $[Zn/Fe] \approx 0$ dex for stars of all metallicity observed within the Galaxy (Sneden et al. 1991). Similarly, the Ni/Fe ratio is significantly lower than metal-poor halo stars, which is consistent with Ni being more heavily depleted than Fe in depleted regions of the ISM. Lu et al. (1996) have argued the underabundance is primarily due to an error in the oscillator strengths for the NiII transitions. While a recent analysis by Zsargó & Federman (1998) indicates the NiII f-values are poorly determined, it is not clear if this can entirely account for the discrepancy between the damped Ly α observations and the metal-poor halo star abundances. For our analysis, we have adopted the updated f-values from Zsargó & Federman (1998) – which does include a decrease in f_{1714} by a factor of 1.34 - yet a significant underabundance of [Ni/Fe] is still apparent. Therefore it is unclear if errors in the oscillator strengths can fully resolve the discrepancy between the observed Ni/Fe pattern and that predicted for Type II SN vields.

In contrast to the top two panels, the middle panels

and the Al/Fe abundance pattern are generally consistent with both dust depletion and Type II SN enrichment. As emphasized by Lu et al. (1996), the overabundance³ of Si/Fe relative to solar is very suggestive of Type II supernovae enrichment (McWilliam 1997). In the case of Si/Fe, the Si overabundance is explained as the result of the overproduction of Si – an α -element relative to Fe in Type II supernovae. Similarly, the Cr/Fe and Al/Fe patterns are consistent with those observed for the metalpoor halo stars. Contrary to the Lu et al. observations, however, we observe an overabundance of Cr/Fe at very low metallicity (for [Fe/H] < -1.5, $\langle [Cr/Fe] \rangle = +0.21$). This result is most likely due to the fact that we are biased to high [Cr/Fe] values at low [Fe/H] because low [Cr/Fe] values would imply Cr⁺ column densities below our detection limit. In one system (Q0149+33) we observe [Cr/Zn] > 0 dex indicating it is essentially undepleted by dust grains. Furthermore, we measure an overabundance of Si relative to Fe in this system ([Si/Fe] = +0.12 dex) which is an indication of a Type II α -enhancement although at a somewhat smaller level than most metal-poor halo stars. Lastly, while the [Al/Fe] measurements are broadly consistent with the abundances observed in metalpoor halo stars, there may be a contradiction at very low [Fe/H]. For halo stars with [Fe/H] < -2 dex, [Al/Fe]< -0.4 dex; McWilliam 1997) yet if anything the damped Ly α systems exhibit [Al/Fe] > 0 dex at this metallicity. This result may ultimately pose a serious challenge to the interpretation of Type II SN nucleosynthetic patterns.

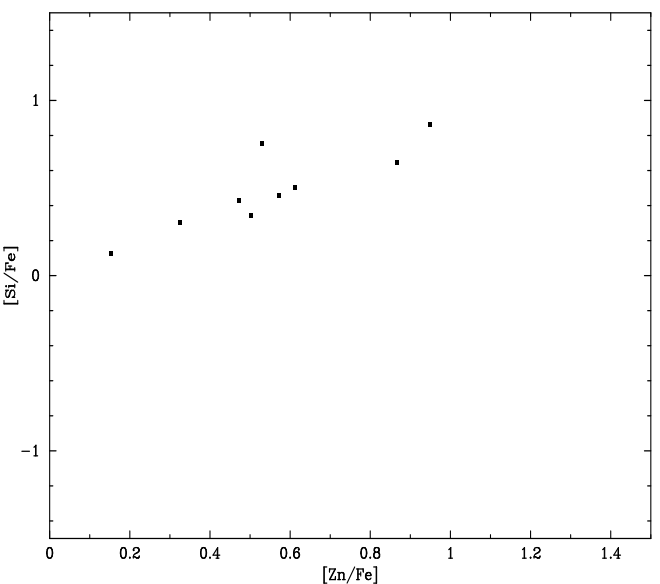


Fig. 23.— [Si/Fe], [Zn/Fe] pairs for the 9 damped Ly α systems from the full sample exhibiting Si, Zn, and Fe. The positive correlation (Pearson's correlation coeffecient r=0.86 with the null hypothesis a 0.003 probability) is suggestie of dust depletion, but could possibly have a nucleosynthetic origin (see text).

While the abundances for Cr, Al and Si vs. Fe resemble those for the metal-poor halo stars, the patterns also tend to match the dust depletion patterns of lightly

 $^3{\rm The}$ one data point with [Si/Fe] <0 is from Q0000–26 where both the Si+ and Fe+ column densities are insecure.

depleted regions within the ISM (Savage and Sembach 1996). In these regions, Si is overabundant relative to Fe, $[Cr/Fe] \approx 0.1$ dex, and recent measurements of the Al to Fe ratio towards three OB stars (Howk & Savage 1998) suggest $[Al/Fe] \gtrsim 0$ dex. If the overabundance of Si/Fe relative to solar is indicative of dust depletion, then one might expect a correlation between [Si/Fe] and [Zn/Fe] with the most heavily depleted regions showing the largest Si/Fe and Zn/Fe ratios. A plot of [Si/Fe] vs. [Zn/Fe] for all the systems with accurate abundances for the three elements (Figure 23) reveals a positive correlation (the Pearson coeffecient is 0.86 in log-space with a null hypothesis probability of 0.003), consistent with that expected for dust depletion. However, if Zn is produced in the neutrino-driven winds of Type II SN (Hoffman et al. 1996), one may also expect a correlation between the abundance of Si and Zn relative to Fe.

Now consider the observations of Ti/Fe (solid squares in the lower right hand panel) which pose a strong argument for Type II SN enrichment. As emphasized in Prochaska & Wolfe (1997a), Ti is more heavily depleted than Fe in dusty regions within the ISM (Lipman & Pettini 1995), yet we find [Ti/Fe] ≥ 0 in every damped Ly α systems where Ti is observed. As Ti is an α -element, this argues strongly for the Type II SN interpretation. Lu et al. (1996) have made similar arguments for the observed underabundance of Mn/Fe in the damped systems. Because Mn is less depleted than Fe in dusty regions of the ISM, the Mn/Fe underabundance cannot be explained by dust depletion. On the other hand one observes [Mn/Fe] < 0 dex for the metal-poor halo stars (McWilliam 1997). Furthermore, the [Mn/Fe] values show a similar trend with [Fe/H] (albeit in terms of an underabundance) to that of the α elements. It is possible this trend indicates a metallicity dependent yield for Mn, but the plateau in [Mn/Fe] values at $[Fe/H] \approx -1$ to -2.5 is better understood if Mn is overproduced relative to Fe by Type Ia supernovae (Nakamura et al. 1998). If the latter explanation is correct, then the low [Mn/Fe] values are significant evidence for Type II SN enrichment within the damped Ly α systems. At the very least, we wish to stress the damped [Mn/Fe] observations require that the underlying nucleosynthetic pattern does not simply match solar abundances.

For the elements considered thus far, the abundance patterns are broadly consistent with a combination of Type II SN enrichment and an 'ISM-like' dust depletion pattern. This is not the case for Sulphur. In the two cases from our full sample where we have accurate measurements for S/Fe we find: (i) [S/Fe] = 0.50 ± 0.02 for the damped system at z = 3.025 toward Q0347-38 and (ii) [S/Fe] = 0.17 ± 0.1 for the damped system toward Q2348-14. Similar to Silicon, Sulfur is an α -element and is observed to be overabundant relative to Fe in metal-poor halo stars by $[Si/Fe]_{II} \approx 0.3 - 0.5$ dex. Like Zinc, Sulfur is undepleted in the ISM. Therefore, interpreting the positive [Zn/Fe] values as the result of dust depletion, one would expect typical values for $[S/Fe]_{dust} > 0.3$ dex on the basis of depletion alone. Given all of the damped systems – including those from Lu et al. (1996) – exhibit $[S/Fe] \leq 0.5$ dex, the S abundance pattern is inconsistent with a combination of Type II SN enrichment and dust depletion because this would require $[S/Fe]_{obs} = [S/Fe]_{II} + [S/Fe]_{dust} > 0.6 \text{ dex}$ in every case. While this point has been discussed previ-

ously, it needs to be emphasized. If dust is playing the primary role in the observed abundance patterns of the damped Ly α systems, then the [S/Fe] measurements require one of two conclusions: (1) the damped Ly α systems were not primarily enriched by Type II SN or (2) all of the systems where S has been measured are atypical in that they are the few which are undepleted. The first conclusion is at odds with most theories of galactic chemical evolution and is inconsistent with the observations of the Milky Way. To adopt point (1), one would have to argue the chemical history of the damped systems is very different from that of the Milky Way. Point (2) is a possibility for Q2348-14, but the Ni/Fe ratio observed for Q0347-38 ([Ni/Fe] < -0.5) would indicate this system is significantly depleted. At present, then, any attempt to match the abundance patterns of the damped Ly α systems with a combination of Type II SN enrichment and ISM-like dust depletion must fail the S observations.

Synthesizing our results with those from previous studies, we contend the abundance patterns of the damped Ly α systems lack any convincing single interpretation. On the face of it this may not be surprising, as one would expect some differences in their chemical evolution. While this would explain variations of a particular X/Fe ratio, this is unlikely to account for any of the inconsistencies discussed thus far. While the majority of the patterns are in excellent agreement with the Type II SN enriched halo star abundance patterns, Zn/Fe and Ni/Fe are clearly inconsistent and are very suggestive of dust depletion, albeit at considerably lower levels than that observed in dusty ISM clouds. An 'ISM-like' dust depletion pattern on top of solar abundances accounts for a majority of the observations but fails for Mn/Fe and Ti/Fe. Attempts to match the observed abundance patterns with a combination of dust depletion and Type II supernovae enrichment have been largely unsuccessful (Lu et al. 1996, Kulkarni et al. 1997, Vladilo 1998). This failure is accentuated by our measurements of [S/Fe] which are inconsistent with a synthesis of dust depletion and Type II SN abundance patterns. Of course to eliminate either effect would have profound consequences. If the damped Ly α systems do not exhibit Type II SN abundances they have a very different chemical evolution history than the Milky Way, in that they do not match the stellar abundance patterns for [Fe/H] < -1 dex. This would beg the questions: Is the Milky Way unique? Or do the damped Ly α systems somehow not include the progenitors of present-day spiral galaxies? Also, why would the damped systems exhibit relative solar abundances for all elements except Mn and Ti? On the other hand, if there is no dust depletion at play, then is the Zn/Fe ratio observed in the Milky Way a special case? Also, are the [Al/Fe] observation at low metallicity consistent with the Type II SN interpretation?

At the heart of these questions lies the physical nature of the damped Ly α systems. If dust depletion is playing a principal role, then perhaps the damped systems are tracing gas-rich galaxies not unlike the Magellanic Clouds (Welty et al. 1997), whereas an underlying Type II SN pattern is more suggestive of the progenitors of massive spiral galaxies. What steps can be taken to resolve these issues? First, the overabudance of Ti/Fe must be confirmed. A more accurate measurement of the TiII 1910 f values would be particularly useful. This could be achieved

by performing observations of a system showing both the TiII 1910 and TiII 3073 transitions. Unfortunately, at present this requires high S/N, high resolution observations at wavelengths exceeding 9000 Å(i.e. $z \approx 2$). One could much more easily measure [Ti/Fe] in a few low z systems via the TiII 3073 transition, but the majority of these systems exhibit [Fe/H] > -1 dex (Pettini et al. 1998) and therefore may not offer a fair comparison with the metalpoor halo stars. It is interesting to note, however, that the presumed damped system at z = 0.75 towards Q2206-19 has [Ti/Fe]= 0.27 dex indicates an underlying Type II SN abundance pattern (Prochaska & Wolfe 1997a). Second, one can look to the relative abundances of the α elements S, Si, O and Ti to investigate consistency with the metal-poor halo star patterns. Thus far the few data points we have are consistent with the Type II SN interpretation ($[S/Si] \approx 0.2$ dex and $[Si/Ti] \approx 0.1$ dex). Third, the conclusions we have drawn from the S/Fe ratio are based on very few damped Ly α systems. Given the importance of this particular ratio, further measurements of Sulphur would be particularly enlightening. Lastly, a more detailed abundance analysis of the lowest metallicity systems would allow one to investigate the chemical evolution of the damped systems. Assuming the extremely metalpoor systems are the least depleted, they should provide the most accurate indication of the underlying nucleosynthetic pattern.

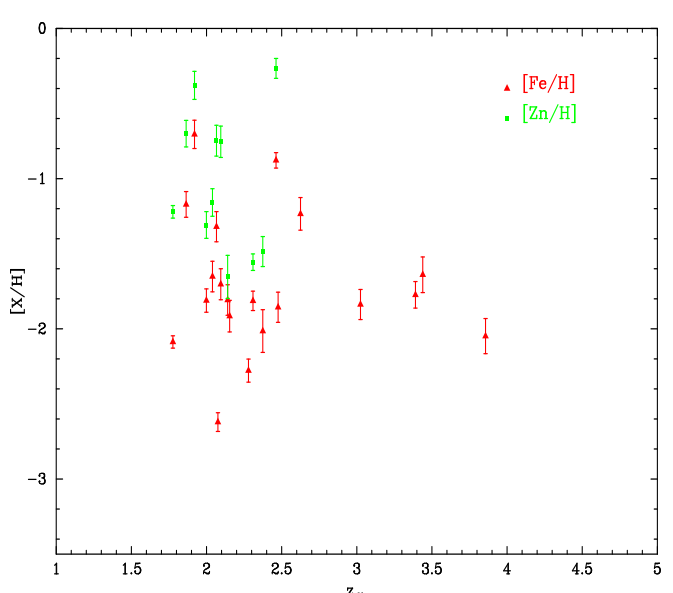


Fig. 24.— [Zn/H] and [Fe/H] measurements from the full sample of damped Ly α systems vs. redshift.

5. METALLICITY

We now turn to examine the metallicity of our sample of damped systems. Given the debate on the presence of dust in the damped Ly α systems, we will consider both Zn/H and Fe/H. Figure 24 plots our complete sample of [Zn/H] and [Fe/H] measurements vs. redshift. The column density-weighted mean for Zn,

$$[\langle \text{Zn/H} \rangle] = \log \frac{\sum_{i} N(\text{Zn}^{+})_{i}}{\sum_{i} N(\text{H}^{0})_{i}} - \log(\text{Zn/H})_{\odot} ,$$
 (2)

for our full sample is $[<\text{Zn/H}>] = -1.15\pm0.15\,\text{dex}^4$. This result confirms that of Pettini et al. (1997). For Fe, we find $[<\text{Fe/H}>] = -1.64\pm0.11\,\text{dex}$ for z<3 and $-1.77\pm0.11\,\text{dex}$ for z>3. Lu et al. (1997) have used similar measurements (in fact several of the values presented here) to conclude that $z\approx3$ marks the onset of significant star formation in the damped Ly α systems. Their interpretation is based on the fact that the damped systems exhibit a break in [<Fe/H>] at $z\approx3$. Formally, our data does not support their conclusion, but the fact that the high redshift [<Fe/H>] value is dominated by only three systems (Q0000–26, Q0019–15, and Q0347–38) suggests our result is probably suffering from small number statistics.

6. SUMMARY AND CONCLUSIONS

We have presented accurate ionic column density and abundance measurements for 19 damped Ly α systems observed with HIRES on the 10m W.M. Keck Telescope. Throughout the paper we have utilized the apparent column density techniques to analyze the damped Ly α profiles and have adopted $N({\rm HI})$ values from the literature. The main results of the paper are summarized as follows:

- 1. The abundance patterns of our 19 systems match those observed by Lu et al. (1996). Therefore, our analysis confirms their primary conclusion that the damped Lyα systems exhibit abundance patterns representative of Type II SN enrichment with the major exception of [Zn/Fe] and to a lesser extent [Ni/Fe]. The Zn and Ni patterns, however, are in accordance with what one would expect for dust depletion based on observations of the lightly depleted, 'warm' HI clouds in the ISM. While the combination of dust depletion and Type II SN enrichment fits the majority of the observations, this interpretation is ruled out by the observed values of [S/Fe].
- 2. A majority of the damped Ly α elemental abundances are consistent with a dust depletion pattern on top of an underlying solar abundance pattern. Observations of Titanium and Manganese, however, strongly contradict this interpretation. In every system where Ti is observed, we measure [Ti/Fe] ≥ 0 dex consistent with the observed overabundance found in metal-poor halo stars and therefore suggestive of Type II SN enrichment. Similarly, the observed underabundance of [Mn/Fe] (Lu et al. 1996) is opposite to the effects of dust depletion and therefore requires a nucleosynthetic explanation, albeit not necessarily Type II SN yields.
- 3. Our metallicity measurements confirm the principal results from the surveys of Pettini and collaborators. Specifically, we find: $[<\text{Zn/H}>] = -1.15 \pm 0.15 \text{ dex}$, $[<\text{Fe/H}>] = -1.64 \pm 0.11 \text{ dex for } z < 3$, and $-1.77 \pm 0.11 \text{ dex for } z > 3$. Although we do not

 $^{^4}$ Note the error estimate reflects the errors in the individual [Zn/H] measurements and not the size of the data sample.

- observe an evolution in the column density-weighted Fe abundance with redshift as claimed by Lu et al. (1997) we expect this inconsistency lies in the small number statistics of our high z sample.
- 4. For a number of damped Ly α systems in our sample (e.g. Q1331, Q0201, Q2348), we observe metal-line systems within 500 km s⁻¹ of the damped system. In the case of Q2348, for example, a metal-line system exhibiting SiII, SiIV and AlIII transitions is located only 100 km s^{-1} from the strongest damped Ly α component. The absence of FeII and OI absorption and the SiII/SiIV ratio for this component, however, indicates this system is significantly ionized. We believe the same is true for the majority of these neighboring metal-line systems (the system at z = 1.858 toward Q2230+02 is a notable exception). If they were identified independently of the damped system, these systems would be very strong Lyman limit systems. Their coincidence with the damped system suggests they lie within the halo enclosing the damped system or perhaps that of a neighboring protogalactic system. We expect a detailed analysis of these systems may provide important insight into the physical conditions surrounding the damped Ly α systems.

We acknowledge very helpful discussions with A. McWilliam, M. Pettini, and G. Fuller. We also would like to thank L. Storrie-Lombardi and I. Hook for helping to provide target lists and $N({\rm HI})$ measurements. We acknowledge the very helpful Keck support staff for their efforts in performing these observations. AMW and JXP were partially supported by NASA grant NAGW-2119 and NSF grant AST 86-9420443.

REFERENCES

- Evardsson, B., Anderson, J., Gutasfsson, B., Lambert, D.L., Nissen, P.E., and Tompkin, J. 1993, Astronomy and Astrophysics, 275,

- 101.
 Fall, S.M. & Pei, Y.C. 1993, ApJ, 402, 479
 Ferland, G. J. 1991, Ohio State Internal Report 91-01
 Hoffman, R.D. et al. 1996, ApJ, 460, 478
 Howk, J.C. & Savage, B.D. 1998, ApJ, submitted
 Kulkarni, V.P., Fall, S.M., & Truran, J.W. 1997, ApJ, 484, 7
 Lipman, K. & Pettini, M. 1995, ApJ, 442, 628
 Lu, L., Sargent, W.L.W., Barlow, T.A., Churchill, C.W., & Vogt, S.
 1996, ApJS, 107, 475
 Lu, L., Sargent, W.L.W., Barlow, T.A., 1997,
 Malaney, R.A. and Chaboyer, B. 1996, ApJ, 462, 57
 McWilliam, Andrew 1997, ARA&A, 35, 503

- McWilliam, Andrew 1997, ARA&A, 35, 503 Morton, D.C. 1991, ApJS, 77, 119
- Nakamura, T., Umeda, H., Nomoto, K., Thielemann, F., & Burrows, A. 1998, ApJ, submitted (astro-ph/9809307)
 Pettini, M., Smith, L. J., Hunstead, R. W., and King, D. L. 1994, ApJ, 426, 79
- Pettini, M., Lipman, K., & Hunstead, R.W. 1995, ApJ, 451, 100 Pettini, M., Smith, L.J., King, D.L., & Hunstead, R.W. 1997, ApJ,
- 486, 665 Pettini, M., Ellison, S., Steidel, C.C., & Bowen, D.V. 1998, ApJ, in
- Prochaska, J. X. & Wolfe, A. M. 1996, ApJ, 470, 403
- Prochaska, J. X. & Wolfe, A. M. 1997, ApJ, 474, 140 Prochaska, J. X. & Wolfe, A. M. 1997, ApJ, 486, 73

- Prochaska, J. X. & Wolfe, A. M. 1998, ApJ, in press Savage, B. D. and Sembach, K. R. 1991, ApJ, 379, 245 Savage, B. D. and Sembach, K. R. 1996, ARA&A, 34, 279
- Songaila et al. 1994, Nature, 371, 43 Sneden, C., Gratton, R.G., & Crocker, D.A. 1991, A & A, 246, 354

- Sneden, C., Gratton, R.G., & Crocker, D.A. 1991, A & A, 246, 354
 Storrie-Lombardi, L.J. & Wolfe, A.M. 1998, in preparation
 Tripp, T. M., Lu L., & Savage B.D. 1996, ApJS, 102, 239
 Viegas, S.M. 1994, MNRAS, 276, 268
 Vladilo, G. 1998, ApJ, 493, 583
 Vogt, S. S. 1992, in ESO Conf. and Workshop Proc. 40,
 High Resolution Spectroscopy with the VLT, ed. M.-H. Ulrich (Garching: ESO), p. 223
- Welty, D.E., Lauroesch, J.T., Blades, J.C., Hobbs, L.M., & York, D.G. 1997, ApJ, 489, 672
 Wolfe, A.M., & Davis, M.M. 1979, AJ, 84, 699
- Wolfe, A.M., To ApJS, 61, 249 Turnshek, D.A., Smith, H.E., & Cohen, R.D. 1986,
- Wolfe, A. M., Lanzetta, K. M., Foltz, C. B., and Chaffee, F. H. 1995, ApJ, 454, 698 Wolfe, A.M. & Prochaska, J.X. 1998, ApJ, 494, 15L
- Zsargó, J. & Federman, S.R. 1998, ApJ, 498, 256

Fig. 3.— Velocity plot of the metal-line transitions for the damped Ly α system at z=2.309 toward Q0100+13. The vertical line at v=0 corresponds to z=2.309.

17

- Fig. 4.— Velocity plot of the metal-line transitions for the damped Ly α system at z=2.141 toward Q0149+33. The vertical line at v = 0 corresponds to z = 2.140755.
- Fig. 5.— Velocity plot of the metal-line transitions for the damped Ly α system at z = 3.025 toward Q0347-38. The vertical line at v = 0 corresponds to z = 3.0247.
- Fig. 6.— Velocity plot of the metal-line transitions for the damped Ly α system at z=2.040 toward Q0458-02. The vertical line at v = 0 corresponds to z = 2.03955.
- Fig. 7.— Velocity plot of the metal-line transitions for the damped Ly α system at z=2.374 toward Q0841+12. The vertical line at v = 0 corresponds to z = 2.374518.
- Fig. 8.— Velocity plot of the metal-line transitions for the damped Ly α system at z=2.476 toward Q0841+12. The vertical line at v = 0 corresponds to z = 2.476219.
- Fig. 9.— Velocity plot of the metal-line transitions for the damped Ly α system at z=3.386 toward Q0951-04. The vertical line at v = 0 corresponds to z = 3.856689.
- Fig. 10.— Velocity plot of the metal-line transitions for the damped Ly α system at z = 4.203 toward Q0951-04. The vertical line at v = 0 corresponds to z = 4.202896.
- Fig. 11.— Velocity plot of the metal-line transitions for the damped Ly α system at z = 1.999 toward Q1215+33. The vertical line at v = 0 corresponds to z = 1.9991.
- Fig. 12.— Velocity plot of the metal-line transitions for the damped Ly α system at z=1.776 toward Q1331+17. The vertical line at v = 0 corresponds to z = 1.77636.
- Fig. 13.— Velocity plot of the metal-line transitions for the damped Ly α system at z = 3.736 toward Q1346-03. The vertical line at v=0 corresponds to z=3.735830.
- Fig. 14.— Velocity plot of the metal-line transitions for the damped Ly α system at z=2.625 toward Q1759+75. The vertical line at v = 0 corresponds to z = 2.6253.
- Fig. 15.— Velocity plot of the metal-line transitions for the damped Ly α system at z = 1.864 toward Q2230+02. The vertical line at v = 0 corresponds to z = 1.864388.
- Fig. 2.— Velocity plot of the metal-line transitions for the damped Ly α system at z=3.439 toward Q0019-15. The vertical line at v = 0 corresponds to z = 3.43866.

Fig. 16.— Velocity plot of the metal-line transitions for the presumed damped system at z=1.859 toward Q2230+02. The vertical line at v=0 corresponds to z=1.858536.

Fig. 17.— Velocity plot of the metal-line transitions for the damped Ly α system at z=2.066 toward Q2231-00. The vertical line at v=0 corresponds to z=2.06615.

Fig. 18.— Velocity plot of the metal-line transitions for the damped Ly α system at z=2.279 toward Q2348–14. The vertical line at v=0 corresponds to z=2.2794.

Fig. 19.— Ly α profile for the damped system toward Q2348–14. The overplotted curves correspond to $N({\rm HI})=20.56\pm0.075.$

Fig. 20.— Velocity plot of the metal-line transitions for the damped Ly α system at z=2.095 toward Q2359–02. The vertical line at v=0 corresponds to z=2.095067.

Fig. 21.— Velocity plot of the metal-line transitions for the damped Ly α system at z=2.154 toward Q2359-02. The vertical line at v=0 corresponds to z=2.153934.

